

Dislocation Effects on the Diffraction Line Profiles from Nanocrystalline Domains



ALBERTO LEONARDI and PAOLO SCARDI

A Pd nano-polycrystalline microstructure was simulated by molecular dynamics, including edge or screw dislocations in one of the 50 grains, so as to produce a realistic model of nanocrystalline domain with line defect. The same crystalline domain was also studied, with or without line defects, as a free-standing, isolated nanocrystal. Atomic coordinates of the selected domain were used to generate powder patterns by means of the Debye scattering equation, and these patterns were used as “experimental” data to test existing methods of line profile analysis in controlled condition, *i.e.*, with known type and density of defects. Results show that the Krivolgaz–Wilkins theory of dislocation line broadening qualitatively agrees with the MD model, but errors can be larger than 50 pct. A critical issue arises from the instability of the Krivolgaz–Wilkins model when all line profile parameters are simultaneously refined: reasonable results can be obtained by fixing or restricting some parameters.

DOI: 10.1007/s11661-015-2863-y

© The Minerals, Metals & Materials Society and ASM International 2015

I. INTRODUCTION

DIFFRACTION line profile analysis (LPA) is extensively used in materials science to gather information on plasticity, to measure the extent of deformation and work hardening, and to characterize nanocrystalline phases (*e.g.*, see References 1, 2 and references therein). Measuring the size of coherently scattering domains is the most common application of LPA, dating back to colloidal metal studies of about one century ago,^[3,4] whereas the approach to determine type and quantity of lattice defects is not only comparatively newer but also well established and popular in applied research, especially in metallurgy.^[1,2,5–7]

Most LPA studies and applications concern X-ray diffraction (XRD) from powder or bulk polycrystalline materials, as this is the most frequent case in metal plasticity studies. Even if traditional methods to determine the concentration of line and planar defects can be found in textbook,^[4,7] the topic is still an object of active research and methodological developments. Despite the broad interest in methods and applications, surprisingly few studies have investigated the validity and general reliability of LPA results. This is probably due to the difficulty in obtaining equivalent evidence from other experimental techniques to validate LPA. For example, it is relatively easy to observe dislocations by transmission electron microscopy (TEM), but a quantification of their density in the range of interest of LPA applied to extensively cold-worked metals ($\rho > 10^{14} \text{ m}^{-2}$) is quite difficult to obtain.^[8]

A viable alternative to assess the validity of LPA is using atomistic simulations to build polycrystalline microstructures. Aggregates of crystalline domains can be produced with controlled shape and size distribution, including known type and amount of lattice defects.^[9,10] Molecular dynamics (MD) can be used to equilibrate the simulated systems, thus providing atomic coordinates of realistic microstructures, which can be used to simulate the corresponding powder pattern by means of the Debye scattering equation (DSE).^[11,12] LPA methods can then be used and tested against the simulated data, which can be considered, to this specific purpose, as equivalent to the experimental data typically collected on plastically deformed materials. So far relatively few papers have explored this approach, and generally using simplified integral breadth methods.^[13,14]

In this study, we focus on the effect of line defects, observed in a nanocrystalline Pd domain inside a cluster of grains providing a realistic environment, to assess the effect of dislocations on the diffraction pattern. While the general validity of the hypotheses underlying the Krivolgaz–Wilkins theory of dislocation line profile broadening^[15–18] is confirmed by the present results, difficulties in the practical use clearly emerge; existing methods based on Wilken’s expressions^[17,18] for peak profile broadening caused by dislocations^[17,18] tend to be unstable when all parameters are freely refined (*i.e.*, allowed to be optimized) against the experimental data, and the complexity of the microstructural effects is also an issue not properly considered by the existing LPA methods.

II. SIMULATED MICROSTRUCTURES AND STRAIN FIELDS

A cluster of 50 randomly oriented Pd grains was created as a realistic environment for a grain (labeled G35) containing dislocations in one of the six

ALBERTO LEONARDI, Post-Doctoral Bursary, and PAOLO SCARDI, Full Professor of Materials Science and Technology, are with the Department of Civil, Environmental and Mechanical Engineering, University of Trento, via Mesiano, 77, 38123 Trento, Italy. Contact e-mail: Paolo.Scardi@unitn.it

Manuscript submitted January 23, 2015.

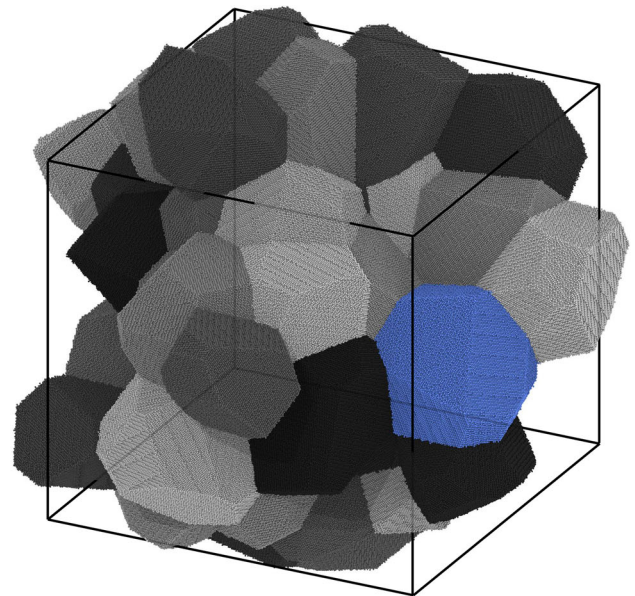
Article published online March 28, 2015

$\{111\}\langle 110 \rangle$ primary slip systems of fcc Palladium (active slip systems are actually twelve considering directions and senses, but the latter are of no interest here). Surrounding grains provide the necessary conditions to stabilize dislocations inside G35, overcoming the strong off-equilibrium condition. Periodic boundary conditions (PBCs) guarantee full immersion of G35 within the microstructure, so that the position of the studied grain is unimportant. Figure 1(a) shows the Pd microstructure after grains crossed by the PBCs have been reconstructed (see below for details). Atomic coordinates of G35, highlighted in the figure, with or without edge or screw dislocations are then used in the DSE^[11,12,19] to generate the powder pattern from a system made of G35 domains with the given type and density of line defects. As shown in the following, this approach allows us to single out the effect of line defects and of grain boundary.^[20]

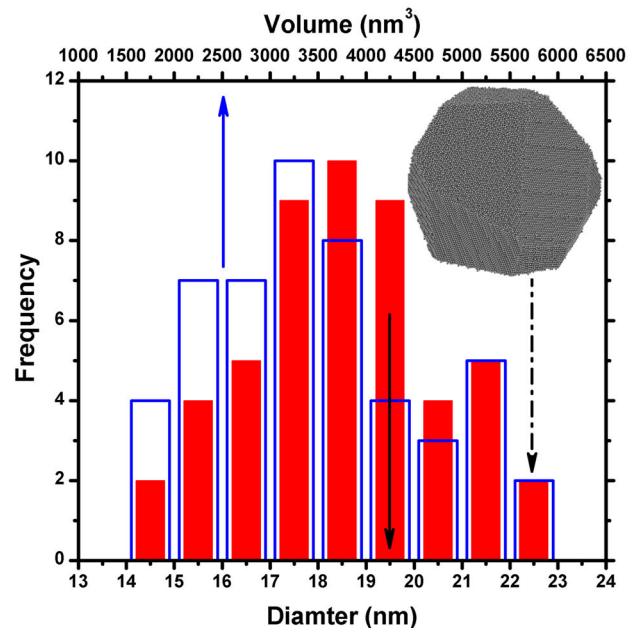
Figure 1(b) shows G35 alone, a further condition studied by MD to highlight the role of the free surface, as opposed to the grain boundary surrounding G35 in the 50 grain microstructure. Simulations were performed on G35 with and without screw dislocations along the six slip systems (Figure 2(a)), both in the microstructure (i) and as an isolated nanocrystalline domain (ii); G35 with an edge dislocation (Figure 2(b)) was also considered (iii), but only when G35 is immersed in the 50 grain microstructure. In fact, the same domain in isolated condition was unstable, with the edge dislocation slipping out of the nanocrystal.

The cluster of grains was generated using a space tessellation algorithm which allows the design of shape and size distribution.^[21,22] Pd grains were built as roughly equiaxial polyhedral, with the volume size distribution shown in Figure 1(b); it also reported the distribution of diameters of spheres with same volume as the polyhedral grains (mean 18.5 nm, standard deviation 2.5 nm). G35 is one of the two largest grains in the microstructure, with an equivalent sphere diameter of 22.3 nm.

After filling up with Pd atoms arranged according to the fcc crystal structure^[21,22] and random misorientation angle distribution (Mackenzie random texture of polycrystal^[23,24]), the microstructure was equilibrated for 1 ns by MD achieving a stable configuration. Large-scale atomic/molecular massively parallel simulator (LAMMPS^[25]) and the embedded atom method (EAM)^[26] with Pd potential of^[27,28] were used, employing a Langevin Nose–Hoover NPT thermostat [constant pressure and temperature of 0 atm and 300 K (27 °C), respectively] and an integration time step of 1 fs. Next to the equilibration, a sequence (time trajectory) of 100 uncorrelated snapshots of the arrangement of atoms in space (frames) was collected at 1 ps time intervals. Finally, the average microstructure was computed over the time trajectory, so as to cancel out any dynamic contribution from the system (e.g., the thermal vibration),^[29] leaving only the static atomic displacement. The latter includes the effect of grain boundary relaxation, as already discussed in similar simulations recently reported in the literature,^[20,29,30] with or without the additional strain field by screw or edge dislocations.



(a)

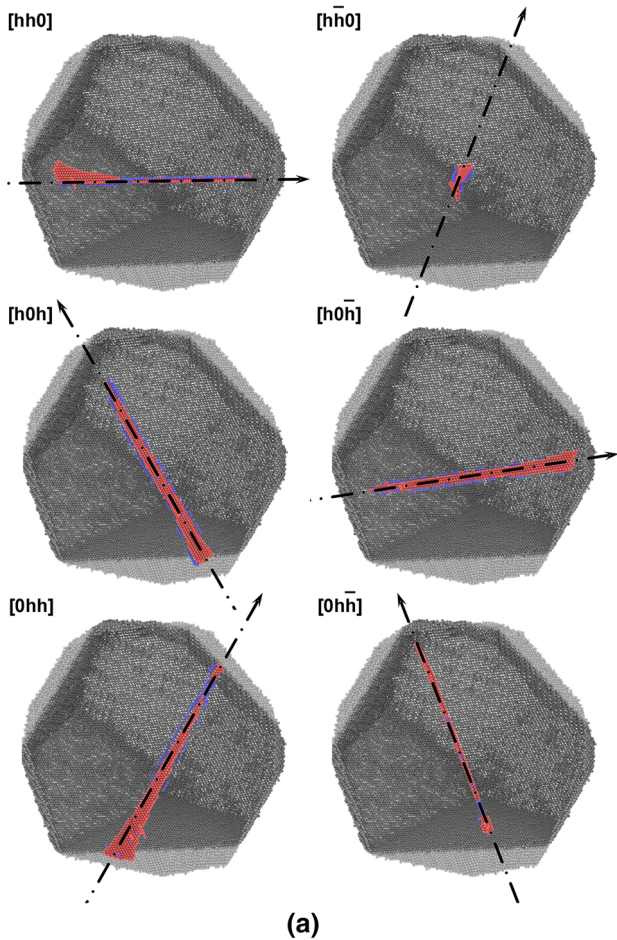


(b)

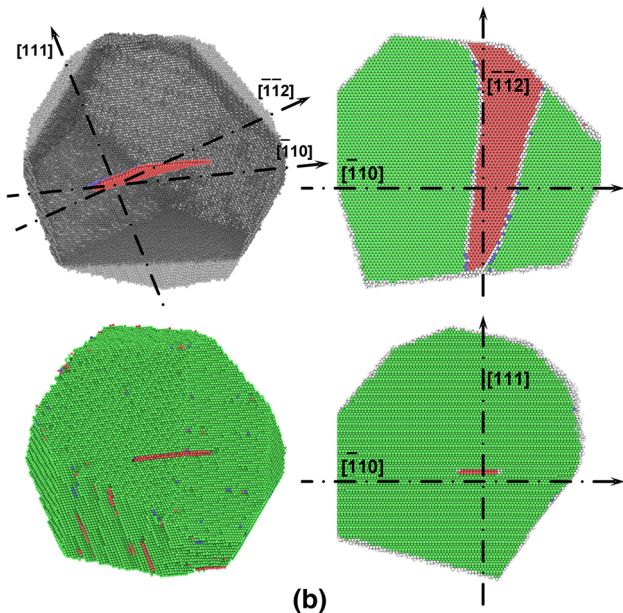
Fig. 1—(a) Simulated Pd microstructure with 50 grains: grains crossed by the PBCs were reconstructed after MD. Grain number 35 (G35), the main object of this work, is highlighted (blue). (b) An isolated G35 is shown, together with the distribution of grain volumes (top abscissa, empty columns) and of diameters of spheres with same volume (bottom abscissa, filled columns) (Color figure online).

As highlighted in Figure 2, dislocations in G35 split in partials according to the expected decomposition reaction^[31]: $\vec{b} = \frac{a}{2}\langle 110 \rangle \rightarrow \vec{b}_p = \frac{a}{6}\langle 121 \rangle$ and $\vec{b}_p = \frac{a}{6}\langle 2\bar{1}\bar{1} \rangle$.

Different from the usual (ideal) assumptions of dislocation theory and continuum mechanics models, MD shows that the separation between partials changes along the dislocation, which also deviates from a straight line (Figure 2). As shown in Figure 3,



(a)



(b)

Fig. 2—G35 with screw dislocations along the six $\langle 110 \rangle$ slip systems (a); G35 with an edge dislocation, as observed along different projections (b). A coordination (Ackland) analysis is used to highlight a region of *hcp* layers (red stripe), which results from the separation in partials of the dislocation line (Color figure online).

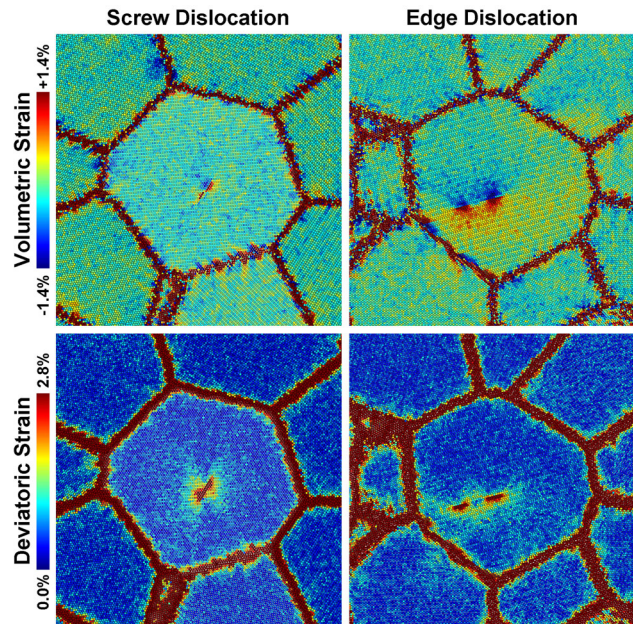


Fig. 3—Strain field in grain G35 with screw (left) and edge (right) dislocations. Strain is mapped on a cross section perpendicular to the dislocation axis; volumetric and deviatoric components are shown for both dislocation types.

the strain field is just qualitatively similar to that of ideal dislocations—screw dislocation with a nearly pure deviatoric field, edge dislocation with compression and tension regions—whereas details differ significantly from the cylindrical symmetry of ideal dislocations. Additional strain components are provided by the grain boundary and the grain–grain interactions,^[20] thus forming a picture quite different from the basic assumptions of the Krivolgaz–Wilkins theory.^[15,16] Figure 4 shows the deviatoric strain in G35 as a function of the radial distance from the dislocation axis. Values provided by MD at different distance were integrated over concentric rings inside the cylindrical volume (with $D \approx 24$ nm) sketched in the same picture. The plot on the right side shows the trend at different heights along the dislocation line, at the center (red) and on top–bottom (near grain boundary) cross sections (blue), respectively. It also shows the expected profile from continuum mechanics for a straight full (unsplit) dislocation (dash-dot, black),^[31] which agrees with the MD predictions just approximately, (i) far from top/bottom surfaces and (ii) in a range of radial distances far from the dislocation core and from the grain boundary region. In fact, MD simulations correctly give no divergence at the dislocation axis, and show the raising component related to the grain boundary strain. Similar considerations hold for G35 containing an edge dislocation. As shown in Figure 2, partial separation is more visible in the edge case, leading to a ribbon of faulted layers along the $[111]$ close packing direction.

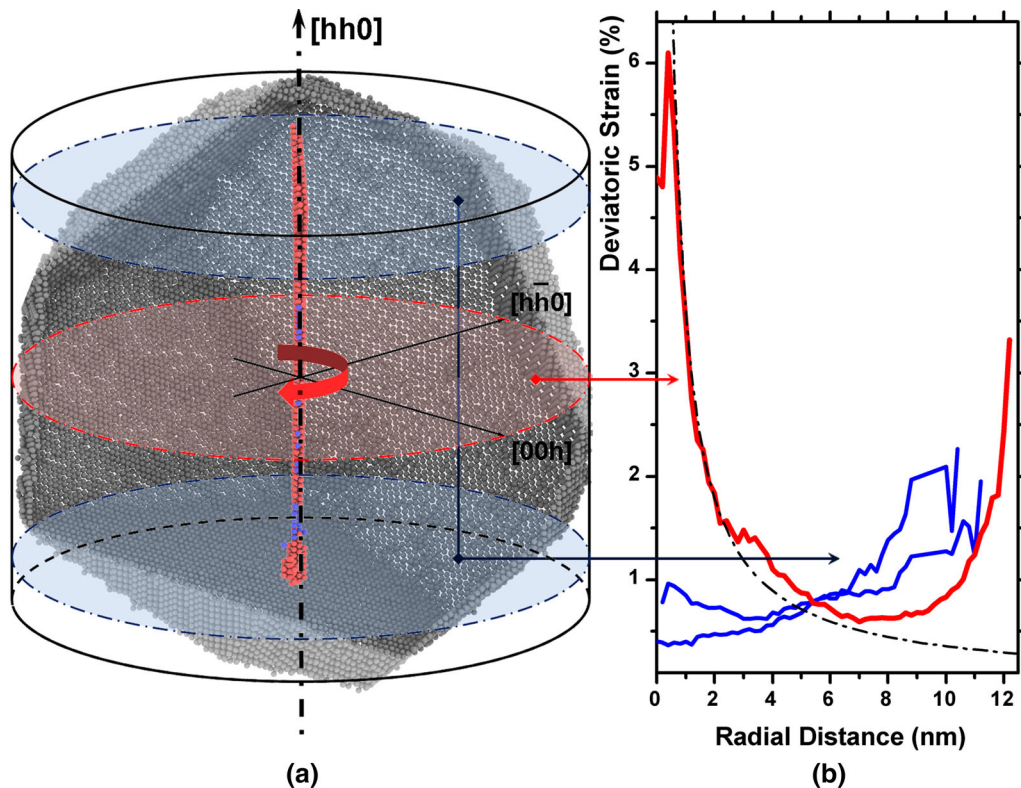


Fig. 4—G35 with screw dislocation (a) and corresponding deviatoric strain (b), obtained from MD simulation as a function of the radial distance from the dislocation axis. Strain values, integrated over concentric rings inside the cylindrical volume sketched around G35, are shown for a cross section through the center (red) and near the top/bottom (blue) of G35. It is also shown the trend of the deviatoric strain for an ideal straight dislocation (dash dot) (Color figure online).

III. POWDER DIFFRACTION PATTERNS FROM MD SIMULATIONS

The results shown so far make us confident that G35 can be considered as a realistic model of nanocrystalline domain in a polycrystal, with or without dislocations, so that the powder diffraction pattern generated by the DSE can be used to assess the validity of existing line profile analysis methods. Figure 5 shows a comparison between the XRD powder pattern generated using the starting (crystallographic) atomic coordinates of G35, and the same G35 grain after MD equilibration inside the 50 grain microstructure, with and without a screw dislocation. MD generally introduces a slight peak shift, as a result of the shrinkage of the starting crystallographic model caused by energy minimization, and a profile broadening, which increases with the scattering vector modulus ($Q = 4\pi\sin\theta/\lambda$); the latter is an expected feature of the introduction of an inhomogeneous strain distribution, due to grain boundary, grain-to-grain interaction and dislocations. The line defect clearly gives the largest contribution, especially visible in the high-angle reflections shown in Figure 5(c).

In Figure 6(a), we compare the powder patterns for G35 each with a screw dislocation along one of the six $\langle hh0 \rangle$ slip systems of Figure 2, with the corresponding average pattern (black line). The difference between the average pattern and each cases is also shown, to highlight the basic fact that, despite morphological

differences in G35 along different $\langle hh0 \rangle$ directions, the strain field—and line broadening induced—by the six slip systems is qualitatively similar, although quantitative differences are to be expected. The average pattern is realistically compatible with the usual assumption that all active slip systems are equally populated. Differences observed in Figure 6(a) clearly stem from the non-spherical shape of G35, which is not a strong feature of the present cluster: larger differences are to be expected for crystalline domains with markedly different cross sections. Figure 6(b) shows a comparison between patterns of G35 inside the polycrystalline cluster, respectively, with screw and edge dislocation. Differences are much larger and more systematic than among the six different slip systems (*cf.* residuals in (a) and (b)), a clear indication of the specificity of the strain field of the different dislocation types.

IV. POWDER PATTERN MODELING

The XRD powder patterns of G35 with the different configurations discussed so far were analyzed by whole powder pattern modeling (WPPM), a state-of-the-art LPA. Full details on WPPM can be found in the literature,^[32,33] with special attention to the study of dislocations.^[34,35] The general philosophy is to model the powder diffraction pattern using line profiles resulting from a convolution of microstructural effects, which

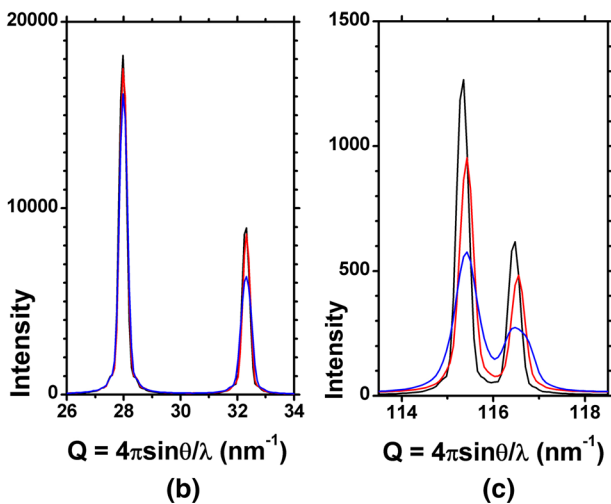
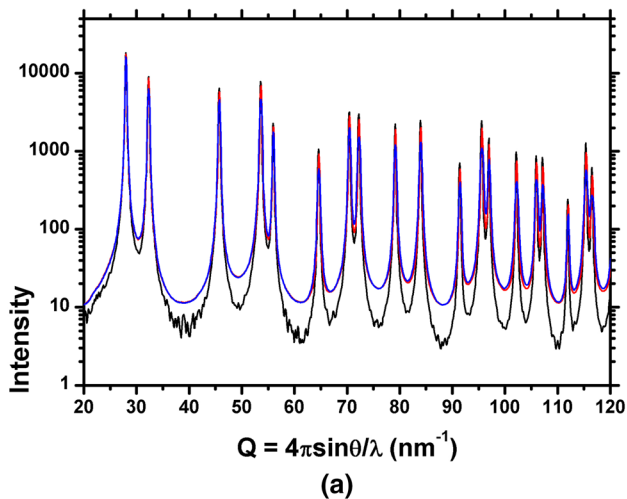


Fig. 5—Comparison of XRD patterns: (a) crystallographic G35 grain (black); G35 in the polycrystalline cluster without (red), and with screw dislocation (blue), both cases after MD. Details of low- and high-angle regions are shown, respectively, in (b) and (c) (Color figure online).

in this specific case are as follows: shape and finite size of the (G35) crystalline domain, the strain field of (screw or edge) dislocations, and an additional grain boundary strain component, which also accounts for the interaction among the 50 grains in the cluster; a low density of planar defects (stacking and twin faults) can also be considered. Details on the algorithm are schematically discussed in the [Appendix](#) and in the cited literature.

For the size effect, we used a recently developed algorithm to calculate the common volume function (CVF) of polyhedral solids.^[36] This allows a nearly perfect modeling of the size broadening effect, which is nicely demonstrated in Figure 7(a) for the powder pattern obtained from the starting (crystallographic) atomic positions of G35. The non-linear least squares (NLLS) minimization (fit) was made using just three refinable parameters, namely the unit cell parameter (a), a domain size scale factor ($dssf$), and an intensity scale factor (isf), being the total number of atoms fixed to the known value of 393,088 which gives a fixed total peak intensity.

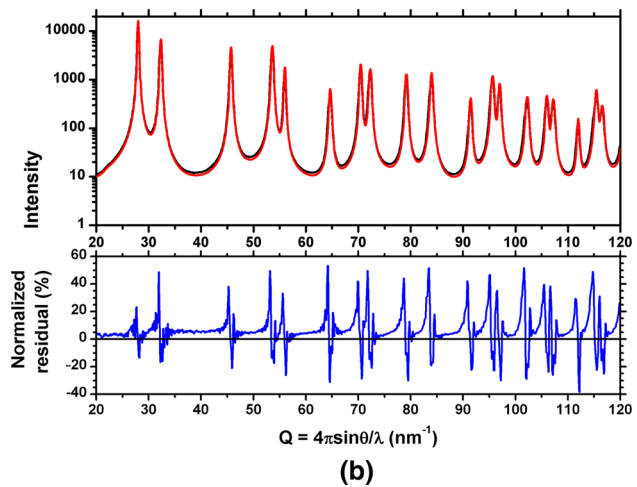
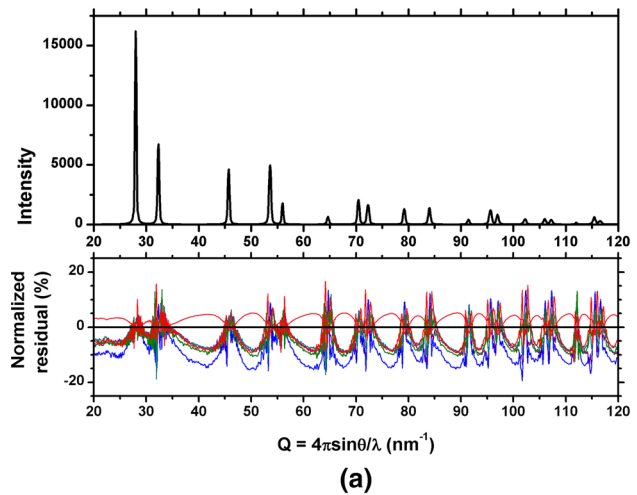


Fig. 6—Average powder pattern after MD of G35 in the polycrystalline cluster, with screw dislocations along the six slip systems (black); the difference between the average pattern and each case is shown as normalized residual (in pct) (a). Powder pattern of G35 in the polycrystalline cluster, with screw (black) and edge (red) dislocation along a randomly chosen slip direction; the difference between the two patterns is shown as normalized residual (in pct) (b) (Color figure online).

The refined unit cell parameter ($a = 0.3890701$ nm) nearly perfectly matches the theoretical value ($a_0 = 0.38907$ nm), whereas $dssf$ (0.99256) and isf (0.99912) are very close but not perfectly matching the nominal values (1 in both cases). This slight mismatch is expected because of the inherently different hypotheses underlying DSE and WPPM, where the former is based on the specific atomistic model of Figure 1, whereas the latter is equivalent to an average of several possible models for the same average polyhedral shape of G35 (see papers by Ino and Minami and related References 37, 38).

This detailed analysis of an apparently obvious result—modeling the pattern of an ideal grain with known size and shape—is to underline the fact that the domain size/shape effect can be accounted for in a nearly perfect way by WPPM when the CVF is available.^[36] In the following modeling, this component of the line profile is fixed, apart from $dssf$ and isf , which

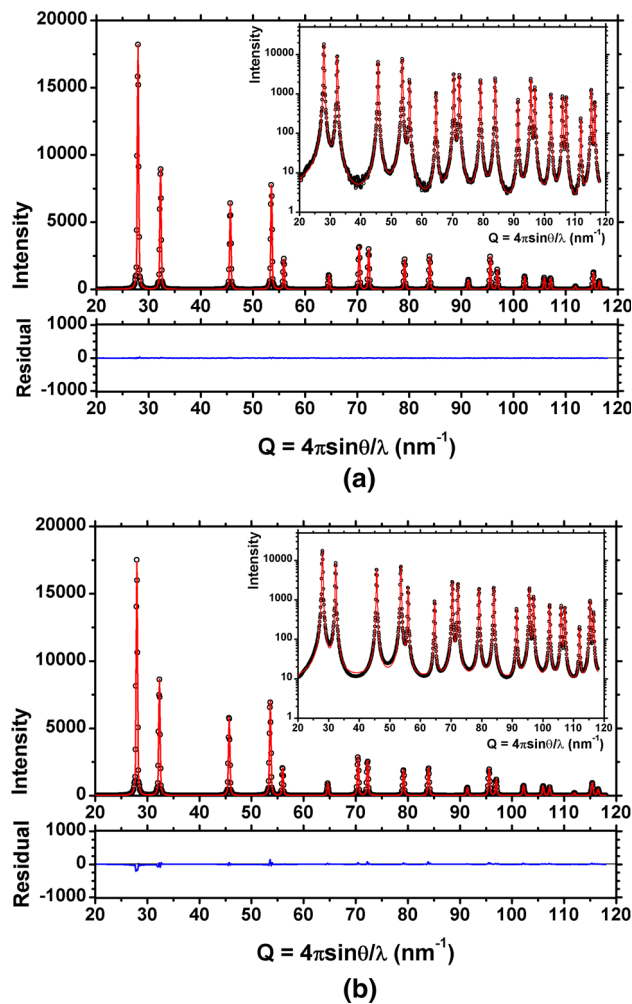


Fig. 7—WPPM result (line) for the powder pattern obtained from the starting (crystallographic) atomic positions of G35 (dot) (a), and the same G35 grain in the polycrystalline system after MD equilibration (b). The difference (residual) is shown below. Insets show corresponding data and fits in log scale.

are allowed to vary slightly, to account for small changes caused by MD.^[20]

As already pointed out, the powder pattern of G35 after energy minimization (Figure 5) includes effects of an inhomogeneous strain due to grain boundaries and grain-to-grain interactions.^[20] Similar effects are also present in the case of an isolated G35 grain, where surface atomic positions are modified by surface tension forces (lower coordination number of surface atoms, causing the so-called surface relaxation effect^[39,40]). We can account for these complex effects, causing a relatively small but measurable strain broadening (or microstrain) component, in a simplified but sufficiently flexible way. According to a modified version of the model proposed by Adler and Houska,^[41–43] the strain distribution can be parameterized according to a Voigtian line profile (see the Appendix) so that the microstrain broadening is modeled just by three fitting parameters, accounting for the intensity and anisotropy of the strain field; the result can be visualized as Warren's plot,^[44] a graphic of the root-mean-square

(rms) displacement $\langle \Delta L^2 \rangle^{1/2}$ (or strain, $\langle \Delta \epsilon^2 \rangle^{1/2} = \langle \Delta L^2 \rangle^{1/2} / L$) as a function of the correlation or Fourier distance (L), inside the crystalline domain for any desired $[hkl]$ crystallographic direction.^[42,43]

As shown in Figure 7(b), this approach (CVF for the size effect and Voigtian line profile for the microstrain effect) gives reasonably good results in terms of fit quality. The analysis shown in Figure 7(b) refers to G35 in the polycrystalline system, after MD equilibration has introduced the grain boundary effects.^[20] Modeling results are equally good for the isolated G35 (not shown here for brevity), where the microstrain is caused by the free surface.^[40,43] Corresponding rms displacement trends are shown in Figure 8(a) (red for G35 in the polycrystalline system, green for isolated G35) for the two extreme behaviors of elastically soft $[h00]$ (line) and elastically stiff $[hhh]$ (dash) directions in the fcc structure of Palladium. As expected, the microstrain is larger for the softer direction; values for the isolated G35 model are lower, but comparable to the case of G35 inside the microstructure.

As shown in Figure 2, crystallographically equivalent screw dislocations can be introduced along six possible directions in G35, corresponding to the $\langle hh0 \rangle$ slip systems. It is then possible to model independently the powder pattern of each case, or to analyze the average pattern. In any case, the powder patterns of G35 with dislocation were modeled together with the corresponding pattern of G35 without dislocation; the latter was used to refine the microstrain caused by the grain boundary (or by the free surface for the isolated G35 models), which was then added to (actually, convolved with) the microstrain caused by dislocations in the modeling of the powder pattern of G35 with line defects. This way—including CVF for the size effect and contribution of microstrain from the surface/grain boundary effects—the effect of dislocation line broadening can be singled out.

For the dislocation line broadening component, which is the main object of our study, we used the Krivoglaž–Wilkins theory of dislocation effects on diffraction line profiles. As detailed in the Appendix and cited references, the theory is based on several parameters related to the dislocation strain field: an average dislocation density (ρ), an effective outer cut-off radius (R_c), the Burgers vector modulus (b), and an average contrast factor (\bar{C}_{hkl}).

The Burgers vector is usually known; being related to the unit cell parameter ($b = a/\sqrt{2}$ for the primary slip system of fcc Pd), which is refined in any case from the peak positions, b is not an additional free parameter. As shown in the Appendix, the contrast factor of fcc Pd can be written as $\bar{C}_{hkl} = A + B \cdot H^2$, where H is a combination of Miller indices, whereas A and B can be calculated for ideal screw and ideal edge dislocations given the slip system and the elastic constants of Pd^[35,42]; unless the anisotropy of the strain field (expressed by B) needs to be refined, also the contrast factor involves no additional free parameters, so that the number of fit parameters is restricted to just two, ρ and R_c . However, it turns out that when ρ and R_c are both freely allowed to vary in the NLLS minimization of

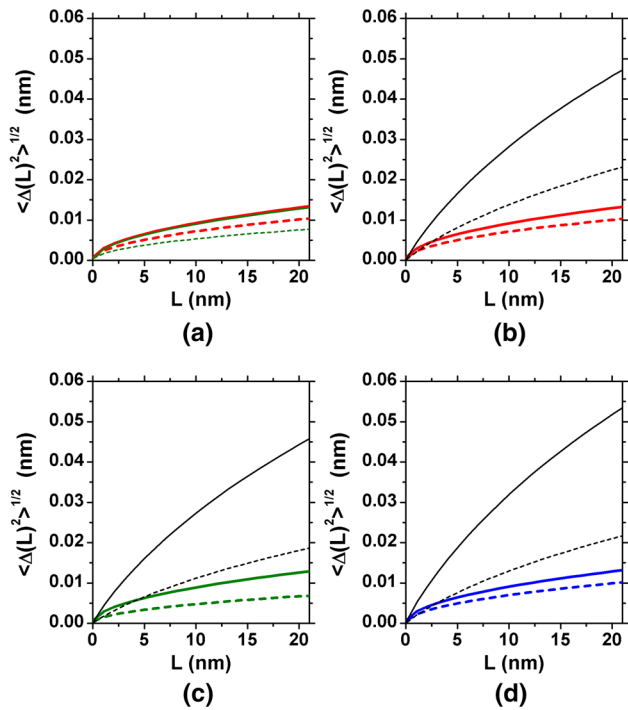


Fig. 8—Warren's diagrams (rms displacement vs L , [111]—dash; [200]—line) for the studied G35 cases, all after MD: without dislocation (a) in the polycrystalline cluster (red) and isolated (green) G35; with screw dislocation (black), G35 inside the polycrystalline cluster (b) and isolated (c); G35 with edge dislocation (d): grain boundary (blue) and dislocation (black) contributions (Color figure online).

patterns of G35 with screw dislocation, the modeling is unstable, with R_e diverging to values $>10^5$ nm. The WPPM quality improves if a small fraction of faults is allowed to be refined, in consideration of the faulted region introduced by the split in partials, but R_e still diverges. Such instability, observed either for individual slip systems or for the average pattern, seems to be an intrinsic problem of Wilkens' model applied to the present case of a screw dislocation in a nanocrystalline domain; it is probably caused by the strong correlation between ρ and R_e , as well as by the difference between the model hypotheses (all based on a concept of ideal, straight, unsplit dislocation) and the real features of the studied system.

Before presenting further results, it is worth discussing the meaning of ρ and R_e in the present context. A nominal value of ρ is provided by the ratio between dislocation line length and volume of G35. This can be taken, from the point of view of the resulting strain field, as an upper limit to the dislocation density (ρ_{\max}), as it does not consider that the grain around the dislocation line is not cylindrical, as the regions invoked by Wilken's theory should be.^[17,18] To illustrate this point, besides the pictures in Figures 2 through 4, it is useful to refer to Figure 9(a), showing the trend of G35 diameter (*i.e.*, the diameter of circles with same area as the cross section) along the screw dislocation axis. The mean diameter in the central region (≈ 18 nm) quickly decays to zero toward the surface (or grain boundary) of G35, with slightly different trends for the different directions corresponding to the six slip systems.

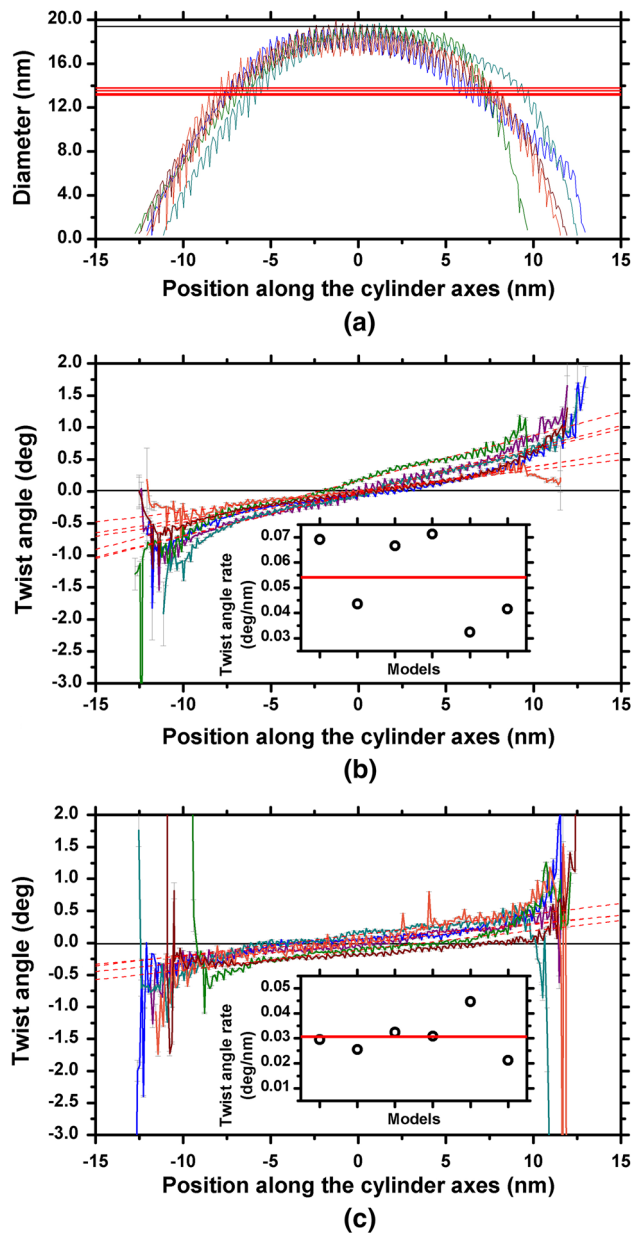


Fig. 9—Cross-sectional diameter of equivalent circle (same area as the cross section) along the axis of the screw dislocation in G35. Trends are shown for the six $\langle hh0 \rangle$ slip system directions (*cf.* Fig. 2), corresponding to dislocation lines of length: 21.51; 22.70; 20.92; 19.72; 21.73; 21.74 (all in nm) (a). Corresponding weighted averages (red line) and cylinder diameter assumed in the Wilkens model (black line) are shown. Twist angle along the screw dislocation axis for G35 as isolated nanoparticle (b) and in the polycrystalline cluster (c); the insets show the rate (in deg/nm) for the six models corresponding to the different $\langle hh0 \rangle$ slip systems. See text for details (Color figure online).

The mean dislocation length is 21.39 nm, with a standard deviation of 1.0 nm; given the volume of G35 (5972.10 nm^3), one easily obtains $\rho_{\max} = 3.58 \times 10^{15} \text{ m}^{-2}$. Based on the values of Figure 9(a), it is also possible to calculate cross-sectional areas along each dislocation line, and then an average value of 298.88 nm^2 , from which an average dislocation density of $\rho_{\text{av}} = 3.33 \times 10^{15} \text{ m}^{-2}$.

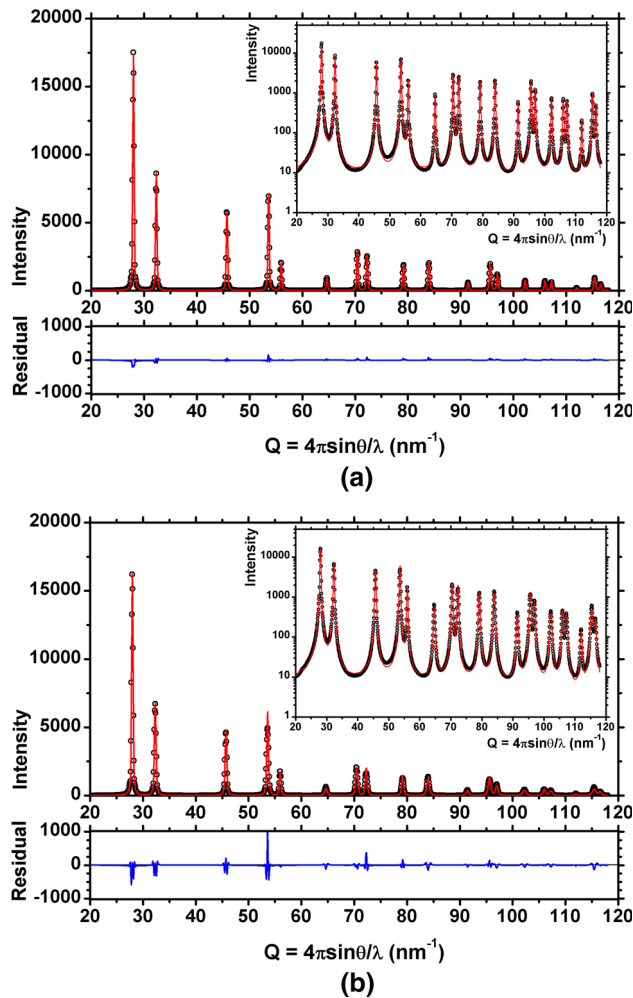


Fig. 10—WPPM result (line) for the average powder pattern (dot) from G35: (a) without screw dislocation, and (b) with screw dislocation along the six slip systems of Fig. 1(a), all after MD. The differences (residuals) are shown below. Insets show same data and fit on log scale.

Similar problems arise for the definition of R_c . According to Wilkens' model, R_c is related to the size of cylindrical regions containing randomly distributed coaxial dislocations.^[18] If a relatively weak $[hkl]$ dependence^[45] is neglected, R_c can be set as approximately equal to twice the radius (R_p) of the regions of restrictedly random distribution of (straight and parallel) dislocations in the material. As a realistic equivalent to the regions of Wilkens, also considering the nearly equiaxial morphology of G35, we can use a cylinder with diameter equal to the height ($D = H$) and same volume as G35, that is $D = H = 19.4$ nm, which gives a dislocation density $\rho_{cyl} = 3.4 \times 10^{15} \text{ m}^{-2}$ (a value in between ρ_{av} and ρ_{max}). We can refer to this equivalent cylindrical domain in the WPPM analysis of powder patterns from G35 with screw dislocation, by setting $R_c = 2R_p = D$. With this realistic assumption, the instability problem in the NLLS minimization is avoided, and the other microstructural parameters can be refined.

As an example, Figure 10 shows the WPPM result for the average powder pattern of Figure 6, and corre-

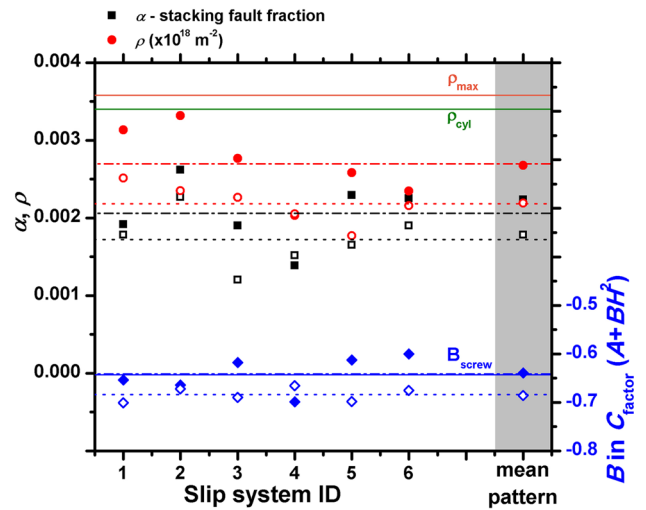


Fig. 11—WPPM results keeping $R_c = D = 19.4$ nm. Dislocation density (circle), deformation fault fraction (square), and B (diamond) in the expression of the contrast factor. Full symbols for the cases of G35 inside the polycrystalline cluster (dash-dot line for mean values of results for the six slip systems); open symbols for the same domain as an isolated object (dot line for mean values of results for the six slip systems). $B_{screw} = -0.643351$ (blue line), expected value for an ideal screw dislocation in Pd; $\rho_{max} = 3.58 \times 10^{15} \text{ m}^{-2}$ (orange line) and $\rho_{cyl} = 3.4 \times 10^{15} \text{ m}^{-2}$ (green line). Results are also shown for the modeling of the mean pattern (gray right side). See text for details (Color figure online).

sponding G35 with no dislocation, both after MD (refined together as explained before). Comparable graphical results are obtained for each case represented in Figures 2 and 6, for G35 both in the polycrystalline cluster and as an isolated (free-standing) grain. Fitting quality is of course lower than in the two cases illustrated by Figure 7 (no dislocations); some structures are present in the residual of Figure 10(b), but the match between DSE data and WPPM can be considered as acceptably good.

The most relevant results are summarized in Figure 11. The refined dislocation density is always smaller than the reference values, ρ_{max} and ρ_{cyl} . Results for the different slip systems scatter about the mean, with values for G35 in the polycrystalline cluster always larger than the corresponding ones in isolated G35 domains. The mean of the results for the six slip systems is nearly identical with the result obtained for the average pattern (in the polycrystalline cluster and as isolated G35 domain), which confirms the validity of the present analysis, and that the average pattern correctly represents the assumption that all slip systems are equally populated. Better results are obtained if a small percentage of faults are added to the WPPM analysis; interestingly, the NLLS keeps to zero the fraction of twin faults, whereas it gives a small but measurable value of stacking faults (see Figure 11), which is compatible with the presence of a small region of stacking fault caused by the split into partial dislocations (*cf.* Figure 2).

It is also possible to verify the type and extent of anisotropy in the line profile broadening by refining B , the hkl -dependent coefficient in the contrast factor (see also the Appendix for details). Refinement results lay

around the expected value of -0.643351 for a screw dislocation in Pd,^[42] while they tend to be slightly smaller in the case of isolated G35 domains.

Microstrain now includes both grain boundary and dislocation contributions, as shown by the Warren's plot in Figures 8(b) and (c), for the average patterns of G35, respectively, in the polycrystalline cluster and isolated. Results for the grain boundary and grain surface contribution are similar to those of Figure 8(a), for G35 without dislocations, whereas dislocations clearly produce a much larger microstrain component. Anisotropy is similar, with elastically soft $[h00]$ (line) and elastically stiff $[hhh]$ (dash) directions, both for the grain boundary/surface and for the dislocation microstrain.

It is worth considering possible reasons for the lower than expected value of dislocation density. Grain shape might have some effect, as the dislocation density and Wilkens' model ideally refer to cylindrical regions, quite different from G35. Further effects might be related to a peculiarity of screw dislocations, originally shown by Eshelby^[46]: a screw dislocation laying along the axis of a cylindrical domain causes a lattice distortion known as Eshelby twist, given by $\alpha = -b/\pi R^2$ (deg/nm), where R is the radius of the cylinder. The strain field tends to relax as an effect of the twist, being thus different from that in an infinite medium. As shown recently, the twist is responsible for a decrease in the microstrain component of diffraction line broadening, which can be seen as an effective decrease in the dislocation density.^[47] In the present case, even if G35 is not cylindrical, and is not free to move or deform in the polycrystalline cluster, the twist is actually present. As shown in Figure 9(b), the twist rate is lower than for a free cylinder of radius $R = D/2 = 19.4/2$ nm ($D = H$ cylinder with same volume as G35), which is $\alpha = -0.053$ deg/nm, and varies for dislocations along the different equivalent $\langle hh0 \rangle$ slip systems. Twist values are variable also in isolated G35 domains with screw dislocation (Figure 9(c)), with an average twist matching the value for the equivalent $D = H$ cylinder. The larger twist observed in the isolated G35 domains is therefore compatible with the lower value of dislocation density refined by the WPPM analysis.

The same analysis made for G35 with screw dislocations can be repeated for edge dislocations. As discussed with reference to Figures 2 and 3, we can only treat the case of G35 in a polycrystalline cluster, as the edge dislocation is not stable in a free-standing, isolated grain, where the atomistic modeling (energy minimization) would lead the line defect out of the crystal. Once we demonstrated that differences among the different $\langle hh0 \rangle \{111\}$ slip systems are relatively small, for brevity, we focused on just one case for the edge dislocation (Figure 2). Here there is no twist, and the deviatoric strain adds to the main volumetric component, with compression/tension regions (Figure 3). Different from the screw case, dislocation partials are visibly separated by a nearly uniform and flat ribbon of stacking fault.

The WPPM analysis simultaneously made on G35 with and without edge dislocation as in previous analyses also gives systematic deviations in the residual and a fit quality comparable to the screw cases. If the

same condition is used on R_e ($R_e = 2R_p = D = 19.4$ nm), the refined dislocation density is $3.4 \times 10^{15} \text{ m}^{-2}$, closely matching the expected ρ_{cyl} value. This result is obtained when faulting is also allowed, and the NLLS procedure gives a 0.004 stacking fault fraction, a value nearly double than that refined in the screw case (cf. Figure 11).

It is worth noting that in the edge case, the dislocation line broadening model is more stable than for the screw case. If ρ and R_e are allowed to vary in the NLLS procedure, both give finite values: $\rho = 2 \times 10^{15} \text{ m}^{-2}$, $R_e = 102$ nm, with a stacking fault fraction of 0.0044, whereas the anisotropy factor $B = -0.70$ (with respect to the expected value for edge dislocations in Pd of -0.474788 ^[42]). So the dislocation density tends to be underestimated, probably as an effect of a too large R_e and B , but refined values make sense. The faulting fraction is equivalent to one fault in ~ 250 layers; G35 has about 90 layers in the $[111]$ stacking direction, so that the faulting value refined by the WPPM analysis corresponds to about 1/3 of layer. Although this is of course just an approximation, as Warren's theory used in the WPPM analysis^[12,32,33] provides for faulted layers crossing the entire crystalline domain, the result seems reasonable in the present context.

V. CONCLUSIONS

The analysis of diffraction data from atomistic simulations proves to be a useful tool to investigate microstructures, and in particular the effect of lattice defects on the diffraction line profiles. As shown in this work, the main contributions to the line profiles can be suitably modeled, including size and shape of the crystalline domain, atomic displacement caused by line defects, grain boundary or surface, and grain-grain interactions, and regions of faulted layer stacking.

The main interest was in the atomic displacement: microstrain effects caused by grain boundary or free surface were accounted for by an effective but flexible Voigtian strain profile model, which also includes anisotropy; dislocation strain was described by the Krivoglaz–Wilkens model, which seems unstable when applied to screw dislocations. Instability is observed when all parameters describing the dislocation effect are simultaneously allowed to vary in data modeling procedures. Reasonable results can be obtained by fixing at least one of the parameters appearing in Wilkens' expression for the Fourier transform (FT) of the dislocation line profile. This possibility was explored considering reasonable values for the effective outer cut-off radius, set equal to the diameter of a cylinder with same volume as the studied nanocrystalline domain ($R_e = D$). While this approach is appropriate to the present context, difficulties might clearly arise in the application to experimental studies, and when more dislocations are present in the same domain.

Even under the most stable conditions (*i.e.*, setting $R_e = D$), and allowing for a small fraction of deformation faults on account of the effect of splitting into partial dislocations, the density of screw dislocations

refined from the powder diffraction data is systematically lower than expected. A large part of this discrepancy was attributed to the Eshelby twist caused by the screw dislocation. Such effect, highest in free-standing (isolated) domains containing screw dislocations, partly relaxes the strain field and is responsible for the apparently lower dislocation density. Interestingly, this effect is present also in the domain inside the polycrystalline aggregate, even if in a minor form, as an effect of the microstructure constraining atomic displacements.

The case of a grain containing an edge dislocation gives better results. If all parameters in Wilken's expression are allowed to be refined in the data modeling, results are incorrect (*e.g.*, dislocation density is underestimated by 50 pct) but make sense (*i.e.*, R_e does not diverges). If the effective outer cut-off radius is constrained as for the screw cases ($R_e = D$), then a good match is found between refined and expected dislocation density. It is also worth noting that, compared to the screw case, the edge dislocation gives no twist but introduces a more extended region of layer faulting, which is also refined to a reasonable value in the data modeling procedure.

APPENDIX

Grain boundary, grain-to-grain interactions, and free surfaces all give quite complex microstrain effects^[20,29,30,42,46] which can be accounted for in a simplified but flexible way using a modified version of a model originally proposed by Adler and Houska,^[41] where the strain distribution is described by a convolution of two Gaussians with different variance (resulting in Voigtian line profiles). The FT of the microstrain peak profile component can then be written as^[42,43,48]

$$A_{\{hkl\}}^D(L) = \exp[-Q^2 L^2 \langle \varepsilon_{hkl}^2(L) \rangle / 2] \\ \cong \exp[-Q^2 \Gamma_{hkl} (aL + bL^2) / 2], \quad [\text{A1}]$$

where Q ($=4\pi \sin\theta/\lambda$) is the wavevector transfer modulus, L is the Fourier length (distance between scattering centers) and $\langle \varepsilon_{hkl}^2(L) \rangle$ is the variance of the strain distribution for a correlation (or Fourier) length L along the given $\{hkl\}$ direction. Anisotropy of the strain field is represented by the corresponding fourth-order invariant form of Miller indices,^[48] which for cubic materials is $\Gamma_{hkl} = 1 + c \cdot (h^2 k^2 + k^2 l^2 + l^2 h^2) / (h^2 + k^2 + l^2)^2 (h^2 + k^2 + l^2)^2 = 1 + c \cdot H^2$. Free (refinable) parameters in Eq. [A1] are then a , b , and c . More details on this approach are provided in References 42, 43.

The expression of the FT for dislocation line broadening is given by Wilkens^[17,18] as

$$A_{\{hkl\}}^{\text{Dis}}(L) = \exp\left[-\frac{b^2}{8\pi} \rho \bar{C}_{hkl} Q^2 L^2 f^* \left(\frac{L}{R_e}\right)\right], \quad [\text{A2}]$$

where ρ is the average dislocation density, b the Burgers vector modulus, and R_e the effective outer cut-off radius, which is related to the extension of the effects of the

dislocation strain field and, more generally, to dislocation interaction. According to Wilkens, R_e is related to the extension of the regions of restrictedly random distribution of straight and parallel dislocations, and is a weakly depending function of the crystallographic direction and Q ^[45]; f^* is a smooth function of L/R_e obtained by Wilkens in a heuristic way, to grant integrability of Eq. [A2].^[18] The average contrast factor, \bar{C}_{hkl} , accounts for the anisotropy of the elastic medium and specific dislocation type and slip system. It depends on crystal symmetry, and more specifically on the Laue group, and can be calculated if elastic tensor components are known, in addition to the dislocation type and slip system. (*e.g.*, see References 34, 35).

The size broadening effect can be treated in a rather general form based on the concept of CVF (aka "ghost" in original papers and books by AJC Wilson^[49]). As shown recently,^[36] the CVF can be obtained for any crystal shape that can be described as a polyhedron, which is also the case of G35 treated in this work. As known from the theory,^[36,49] the CVF, in normalized form, $A_{\{hkl\}}^S(L)$, is the FT of the line profile component generated by domains with the specific size and shape. Once the CVF is known, as for G35, it is possible to produce the powder pattern and also refine the size of the nanocrystal, including a distribution of sizes, which is a possibility not used in the present work. The FT of the total line profile can then be written as follows:

$$A(L) = A_{\{hkl\}}^S(L) A_{\{hkl\}}^D(L) A_{\{hkl\}}^{\text{Dis}}(L), \quad [\text{A3}]$$

which is the basic expression of the WPPM analysis used in this work.

REFERENCES

1. R.L. Snyder, J. Fiala, and H.J. Bunge: *Defect and Microstructure Analysis by Diffraction*, Oxford University Press, Oxford, 1999.
2. E.J. Mittemeijer and P. Scardi, eds.: *Diffraction Analysis of Materials Microstructure, Volume 68 of Springer Series in Materials Science*, Springer, Berlin, 2004.
3. P. Scherrer: *Nachr. Ges. Wiss. Gott. Math. Phys. Kl.*, 1918, vol. 26, p. 98.
4. H.P. Klug and L.E. Alexander: *X-ray Diffraction Procedures for Polycrystalline and Amorphous Materials*, Wiley, New York, NY, 1974.
5. A.R. Stokes and A.J.C. Wilson: *Proc. Phys. Soc. Lond.*, 1944, vol. 56, pp. 174–81.
6. G.K. Williamson and W.H. Hall: *Acta Metall.*, 1953, vol. 1, pp. 22–31.
7. B.E. Warren: *Prog. Met. Phys.*, 1959, vol. 8, pp. 147–202.
8. I. Gutierrez-Urrutia and D. Raabe: *Scripta Mater.*, 2012, vol. 66, pp. 343–46.
9. K.W. Jacobsen and J. Schiøtz: *Nat. Mater.*, 2002, vol. 1, pp. 15–16.
10. A. Stukowski, K. Albe, and D. Farkas: *Phys. Rev. B*, 2010, vol. 82, pp. 224103-1–3-9.
11. P. Debye: *Ann. Phys.*, 1915, vol. 351, pp. 809–23.
12. B.E. Warren: *X-ray Diffraction*, Addison-Wesley, Reading, MA, 1969.
13. P.M. Derlet, S. Van Petegem, and H. Van Swygenhoven: *Phys. Rev. B*, 2005, vol. 71, p. 024114.
14. S. Brandstetter, P.M. Derlet, S. Van Petegem, and H. Van Swygenhoven: *Acta Mater.*, 2008, vol. 58, pp. 165–76.
15. M.A. Krivoglaз and K.P. Ryaboshapka: *Fiz. Metall.*, 1963, vol. 15, pp. 18–28.

16. M.A. Krivoglaz: *Theory of X-ray and Thermal Neutron Scattering by Real Crystals*, Plenum Press, New York, 1969.
17. M. Wilkens: *Phys. Status Solid. A*, 1970, vol. 2, pp. 359–70.
18. M. Wilkens: *Fundamental Aspects of Dislocation Theory*, J.A. Simmons, R. de Wit, and R. Bullough, eds., National Bureau of Standards (US) Special Publication No. 317, NBS, Washington, DC, vol. II, pp. 1195–1221.
19. L. Gelisio, C.L. Azanza Ricardo, M. Leoni, and P. Scardi: *J. Appl. Crystallogr.*, 2010, vol. 43, pp. 647–53.
20. A. Leonardi, M. Leoni, and P. Scardi: *J. Appl. Crystallogr.*, 2013, vol. 46, pp. 63–75.
21. A. Leonardi, M. Leoni, and P. Scardi: *J. Comput. Mater. Sci.*, 2013, vol. 67, pp. 238–42.
22. A. Leonardi, M. Leoni, and P. Scardi: *Philos. Mag.*, 2012, vol. 92, pp. 986–1005.
23. J.K. Mackenzie: *Biometrika*, 1958, vol. 45, pp. 229–40.
24. A. Morawic: *J. Appl. Crystallogr.*, 1995, vol. 28, pp. 289–93.
25. S. Plimpton: *J. Comput. Phys.*, 1995, vol. 117, pp. 1–19.
26. M.S. Daw and M.I. Baskes: *Phys. Rev. B*, 1984, vol. 29, pp. 6443–53.
27. S.M. Foiles, M.I. Baskes, and M.S. Daw: *Phys. Rev. B*, 1986, vol. 33, pp. 7983–91.
28. H.W. Sheng, M.J. Kramer, A. Cadien, T. Fujita, and M.W. Chen: *Phys. Rev. B*, 2011, vol. 83, p. 134118.
29. A. Leonardi, K.R. Beyerlein, T. Xu, M. Li, M. Leoni, and P. Scardi: *Z. Kristallogr. Proc.*, 2011, vol. 1, pp. 37–42.
30. A. Leonardi, M. Leoni, and P. Scardi: *J. Nanosci. Nanotechnol.*, 2012, vol. 12, pp. 8546–53.
31. D. Hull and D.J. Bacon: *Introduction to Dislocations*, Butterworth-Heinemann, Oxford, 1965.
32. P. Scardi and M. Leoni: *Acta Crystallogr. A*, 2002, vol. 58, pp. 190–200.
33. P. Scardi: *Powder Diffraction: Theory and Practice, Chap. XIII*, The Royal Society of Chemistry, Cambridge, U.K., 2008, pp. 376–413.
34. M. Leoni, J. Martinez-Garcia, and P. Scardi: *J. Appl. Crystallogr.*, 2007, vol. 40, pp. 719–24.
35. J. Martinez-Garcia, M. Leoni, and P. Scardi: *Acta Crystallogr. A*, 2009, vol. 65, pp. 109–19.
36. A. Leonardi, M. Leoni, S. Siboni, and P. Scardi: *J. Appl. Crystallogr.*, 2012, vol. 45, pp. 1162–72.
37. T. Ino and N. Minami: *Acta Crystallogr. A*, 1984, vol. 40, pp. 538–44.
38. K.R. Beyerlein, R.L. Snyder, and P. Scardi: *J. Appl. Crystallogr.*, 2011, vol. 44, pp. 945–53.
39. M. Leoni and P. Scardi: *Diffraction Analysis of the Microstructure of Materials, Chapter XVI*, Springer, Berlin, 2004, pp. 413–52.
40. L. Gelisio and P. Scardi: *Metall. Mater. Trans. A*, 2014, vol. 45A, pp. 4786–95.
41. T. Adler and C.R. Houska: *J. Appl. Phys.*, 1979, vol. 50, pp. 3282–87.
42. A. Leonardi and P. Scardi: *Front. Mater.*, 2015, vol. 1, p. 37.
43. P. Scardi, A. Leonardi, L. Gelisio, M.R. Suchomel, B.T. Sneed, M.K. Sheehan, and C.-K. Tsung: *Phys. Rev. B*, 2015, in press.
44. B.E. Warren and B.L. Averbach: *J. Appl. Phys.*, 1950, vol. 21, pp. 595–99.
45. N. Armstrong, M. Leoni, and P. Scardi: *Z. Kristallogr. Suppl.*, 2006, vol. 23, pp. 81–86.
46. J.D. Eshelby: *J. Appl. Phys.*, 1953, vol. 24, pp. 176–79.
47. A. Leonardi, S. Ryu, N. Pugno, and P. Scardi: *J. Appl. Phys.*, 2015, submitted.
48. N.C. Popa: *J. Appl. Crystallogr.*, 1998, vol. 31, pp. 176–80.
49. A.J.C. Wilson: *X-ray Optics: the Diffraction of X-rays by Finite and Imperfect Crystals*, Methuen, London, 1962.